CHAPTER 6
POOL BOILING HEAT TRANSFER ON MICRO-FINNED SURFACES IN SATURATED FC-72

The studies in Chapters 4 and 5 are associated with the pool boiling heat transfer on mini finned surface to prescribed geometric parameters such as fin length and fin spacing. They bring out some unusual boiling characteristics of orientations. In present chapter, a pool boiling experiment is also employed to investigate the boiling heat transfer performance including the boiling incipience superheat, heat transfer coefficient, and critical heat flux of micro-finned surfaces immersed in the dielectric fluid FC-72 with different fin length and orientations. The 10×10 micro fin array with one fin width of 0.5mm and one fin spacing of 0.5mm which fabricated on the 10mm×10mm base area. The fin lengths are designed in 0.5mm, 1.0mm and 2.0mm. Moreover, the direct visual observation is also used to observe the flow patterns of the bubbles in order to understand the boiling heat transfer mechanism in micro structures.

6.1 Visual Flow Pattern Observation of Micro-Finned Surface

Flow pattern observations for saturated dielectric fluid FC-72 boiling on micro-finned surfaces in horizontal orientation are presented in Figure 6.1 to 6.6 with increasing the heat flux from 3×10^{3} Wm^{-2} to 7.5×10^{5} Wm^{-2}. As shown in Figure 6.1, the flow pattern at the boiling incipience is similar to the mini finned surfaces discussed in the previous chapter 4 in which bubbles are mostly generated with the constant rate from the active nucleate sites at the fin tip. However, it is also observed that some nucleate sites at the fin base are activated. For a little more rise in the heat flux values as shown in Figure 6.2, the number of active nucleate sites increase and vertical coalescence of bubbles is observed at some fin tips. Moreover, the small vapor slugs or deformed bubbles at the fin base the inside the fin spacing is also observed in three different test surfaces. Figure 6.3 shows the bubbly flow when the heat flux is in the low heat flux region. Obviously, Figure 6.3(c) shows a different flow pattern inside the spacing of

high finned surface in which the bubbles interact and coalesce with each other. This indicates that bubble departure behaviors inside higher fin array contribute more suppression than that inside the lower arrangement at low heat flux region. At the moderate heat flux region, the fin spacing is filled with the coalesced bubbles and vapor columns are observed for the three test surfaces in Figure 6.4. The interactions of coalesced bubbles or vapor columns might induce larger flow resistance to themselves for the departing movement from the fin array and might obstruct the re-wetting liquid from the perimeter of the test surface. It should be mentioned that at high fin surface as shown in Figure 6.4(c), some vapor mushrooms are formed because of the more violent vapor interactions between the fins. In the high heat flux regions as shown in Figure 6.5, large vapor mushrooms are observed in all test surfaces. Moreover, bubbles coalesce together more frequently and big oscillations and deformations in mushroom shapes are often seen. Finally, as the heat flux is raised further to approach the CHF, a violent and periodical departure behavior of the large vapor mushroom clouds are observed in Figure 6.6. Compared with photographs taken from the mini finned surfaces in Chapter 4, the liquid/vapor exchange mechanism in the present experiment shows a different behavior in which only a few vapor clusters are extruded from the fin spacing. The entire finned surface is enveloped under large vapor mushrooms and come closer to the dry-out situation in the central portion of the finned surface with wall superheat increases.

Figure 6.7 to 6.10 illustrate the flow patterns of the micro-finned surface boiling at vertical orientation. From the photographs in Figure 6.7, initial bubbles are generated from some downward-facing surfaces of the fins for all vertical micro-finned surfaces. This phenomenon is due to the flow resistance by the fins where the superheated liquid is accumulated on the downward-facing surface. As the heat flux increases, the boiling region gradually spreads out the entire finned surface. The departure behavior of the bubbles is quite chaotic and violent on the three test surfaces as shown in Figure 6.8. In Figure 6.8(c) the vapor

clusters are even observed because of the very narrow fin spacing where bubbles coalesce to large one. In moderate heat flux region, the coalescence of bubbles is more significant especially on the test surfaces with fin length 1mm and 2mm as shown in Figure 6.9. Compared with the flow patterns in chapter 5, it can be reasoned that the denser vertical fin array may induce earlier decay in heat transfer performance due to the early vapor clusters will be formed and covered the heating surface. In the high heat flux region as seen in Figure 6.10, the entire finned surface is covered with the vapor mushroom clouds. This phenomenon may cause the re-wetting liquid exhausted and may produce the dry-out situation.

6.2 The Effects of Fin Length for Micro-Finned Surfaces Boiling in Saturated FC-72

The nucleate boiling curves of the micro-finned surfaces with various fin lengths of 2 mm, 1 mm, and 0.5 mm at horizontal and vertical orientations are schematically shown in Figures 6.11 and 6.12. The plots show that the boiling incipience superheat of micro-finned surfaces are relatively low 3.3~7.2K for horizontal orientation and 3.1~5.9K for vertical orientation. Moreover, the data also show that the temperature excursions of boiling curves on the present micro-finned surfaces are quite unapparent. Compared with the incipience superheat and temperature excursion of the mini surfaces in chapter 4, the present data are significantly lower than those of mini finned surface arrangements which indicate that boiling incipience superheat is affected by the higher superheated liquid caused by larger flow resistance in the more compact fin array.

The pool boiling heat transfer coefficient with heat flux for various fin length are plotted in Figure 6.13 and 6.14 with horizontal and vertical orientation respectively. In the low heat flux regime of the boiling curves, the differences among the different finned arrays are negligible. At high heat flux regime, however, lower fin length surface appear to work slightly better, particularly in proximity to the moderate heat flux.

In Figure 6.13 and 6.14 the values of overall heat transfer coefficient versus heat flux are plotted. The boiling data show a typical maximum trend, which evidences a decline in heat transfer effectiveness at higher heat flux region. The trend with a maximum can be explained by the fact that boiling intensifies as the heat flux rises, becoming gradually more efficient until large clusters and accumulations of vapor form among the fins; at this point, the overall heat transfer coefficient begins to decline. The maximum value of the overall heat transfer coefficient depends on the fin length.

The effect of increasing fin length is always a reduction in overall heat transfer coefficient, but this effect is more marked for higher fins. Overall heat transfer coefficient is greater for surfaces with lower fin length. Thermal conduction along lower fins is more effective, and the residence time of the bubble is reduced owing to the effect of the bubble departure path inside lower fin array; therefore, when fin length is decreased, better flow conditions occur and the wetting of the surface by the fluid is made easier, as suggested by Rainey and You [15]. In addition, it can be observed that the early decline for overall heat transfer coefficients on high fin length arrangements at low heat flux region and rapidly decline for overall heat transfer coefficient on low fin length surface at moderate heat flux region.

The mini-finned surfaces with the same fin spacing of 0.5mm and fin lengths (0.5mm, 1.0mm and 2.0mm) are also plotted in Figure 6.13 and 6.14 for comparing the effect of fin width. It is clearly noted that the test surfaces with larger fin width provide higher overall heat transfer coefficient in low and moderate heat flux regions in both orientations. However, early decline and lower overall heat transfer coefficient is also observed in the same test surfaces. This phenomenon can be ascribed to the fact that larger flow resistance to re-wetting liquid due to the micro-finned surfaces have much more fin gap and result worse overall heat transfer coefficient in low and moderate heat flux regions. As the heat flux approaches to the CHF, the heating surface is covered with vapor mushrooms. The test surfaces with larger fin width might

trap the residual vapor in larger adjacent and opposing walls lead to early decay and lower overall heat transfer coefficient.

6.3 The Effects of Orientation for Micro-Finned Surfaces Boiling in Saturated FC-72

The boiling heat transfer coefficients of the horizontal and vertical micro-finned surfaces versus imposed heat flux are plotted in Figure 6.15. The boiling curves of the micro-finned surfaces are affected by the orientation arrangement in high heat flux regime. This figure shows for high fin length surfaces at high heat flux region, the boiling heat transfer coefficient is comparable. However, for high fin length surfaces, there is a negligible difference of nucleate boiling at low and moderate heat flux region. Besides, for low fin length surface, the overall heat transfer coefficient of surface in vertical orientation is better than that in horizontal orientation but reversed in high heat flux region.

6.4 Conclusion Remarks

Experimental investigation of boiling heat transfer phenomena for micro-finned surfaces immersed in saturated FC-72 at an atmospheric pressure subject to horizontal and vertical orientations gives the following results:

1. The boiling incipience superheat of micro-finned surfaces is relatively low for both horizontal and vertical orientations and the temperature excursions of boiling curves are quite unclear. The incipience superheat and temperature excursions of micro-finned surfaces are significantly lower than those of mini finned arrangements.
2. The level-off behavior in overall heat transfer coefficient is observed in the micro-finned surface with the fin length of 2mm unlike the same behavior observed in the mini finned with the fin length of 4mm due to the flow resistance in the micro-finned surface is larger than that in the mini finned surface.

3. The effect of increasing fin length is always a reduction in overall heat transfer coefficient, but this effect is more marked for higher fins. Overall heat transfer coefficient is greater for surfaces with lower fin length.
4. Comparison of horizontal and vertical micro-finned surfaces revealed that while the heat transfer performance in the high heat flux region is higher for the vertical micro-finned surfaces. However, the overall heat transfer coefficient in the fully developed nucleate boiling region was close to each other. The critical heat flux is lower for the vertical micro-finned surfaces.

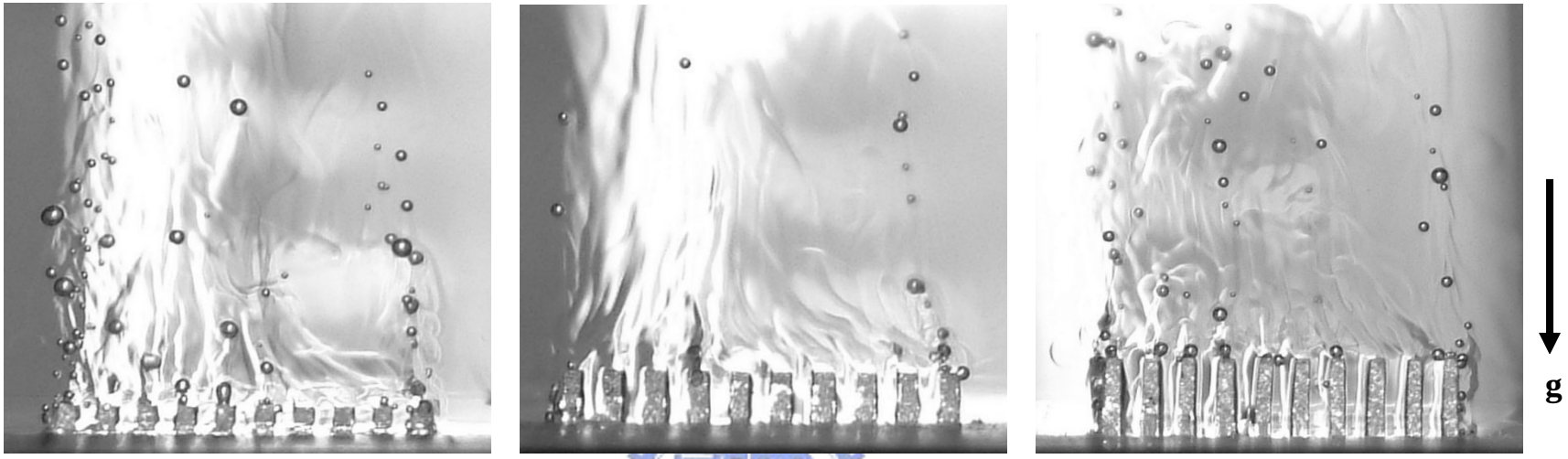

(a) L=0.5mm, 2.6% of CHF (b) L=1.0mm, 1.8% of CHF (c) L=2.0mm, 1.4% of CHF

Figure 6.1 Flow patterns of horizontal micro-finned surfaces with 3 different fin lengths at boiling incipience.

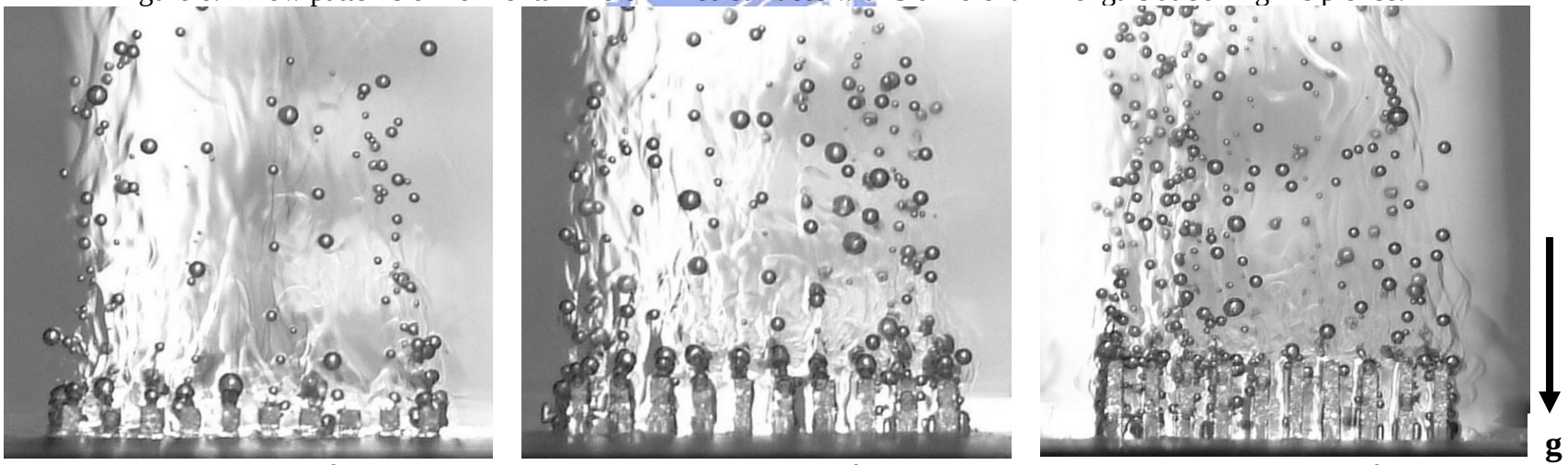

(a) L=0.5mm, 13.3% of CHF (b) L=1.0mm, 14.9% of CHF (c) L=2.0mm, 14.8% of CHF

Figure 6.2 Flow patterns of horizontal micro-finned surfaces with 3 different fin lengths at low heat flux region.

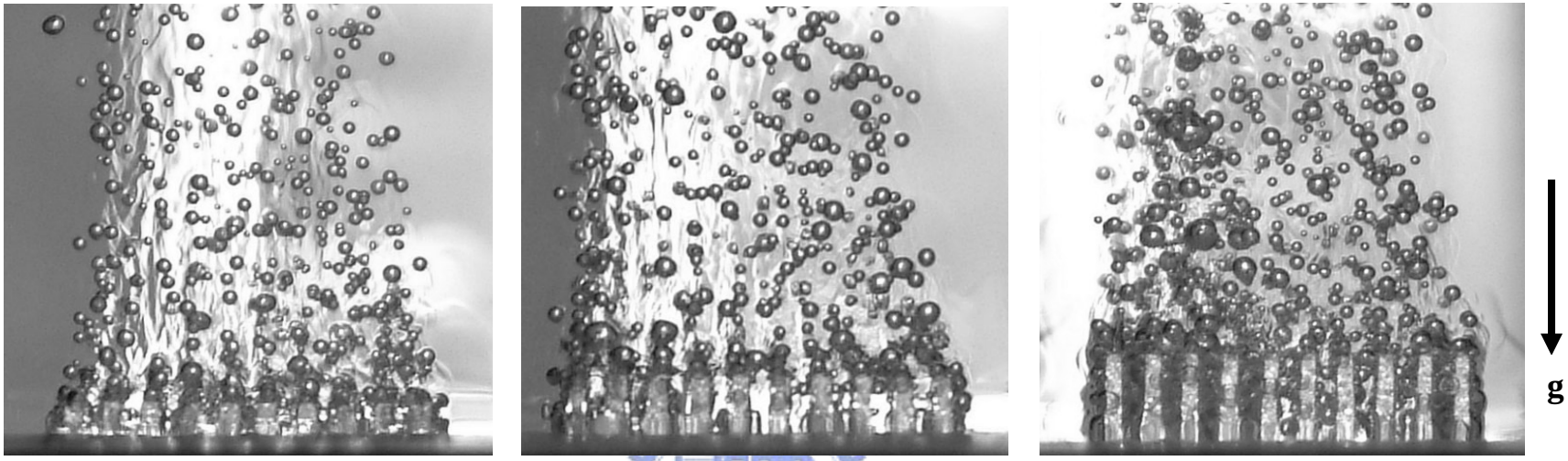

(a) L=0.5mm, 30.4% of CHF (b) L=1.0mm, 33.2% of CHF (c) L=2.0mm, 33.9% of CHF

Figure 6.3 Flow patterns of horizontal micro-finned surfaces with 3 different fin lengths at low heat flux region.

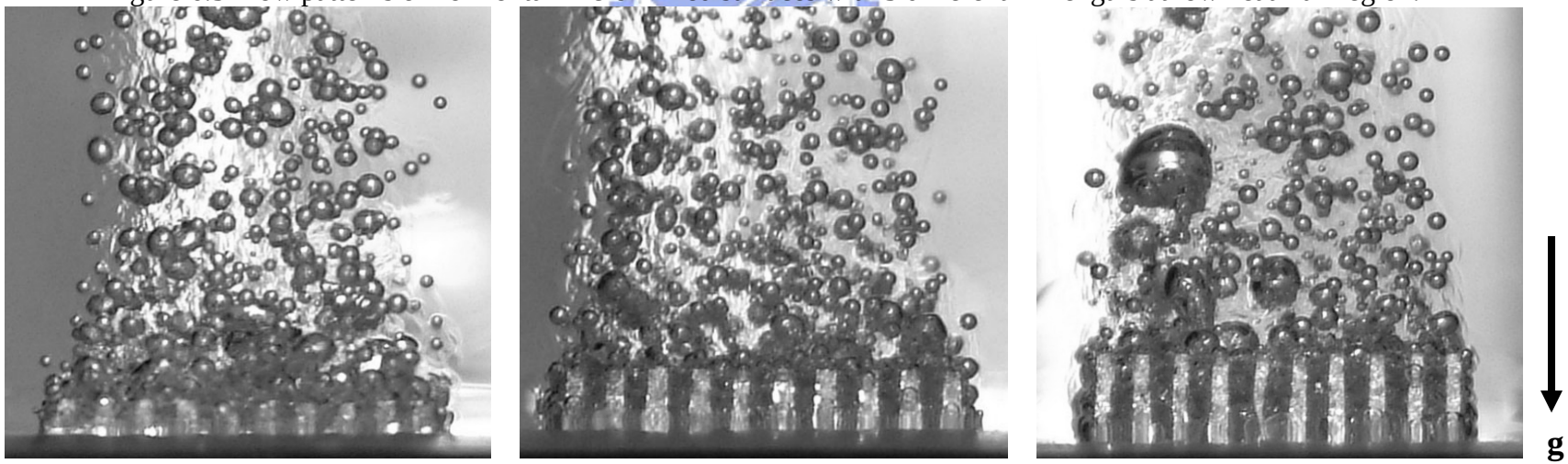

(a) L=0.5mm, 51.3% of CHF (b) L=1.0mm, 50.6% of CHF (c) L=2.0mm, 49.5% of CHF

Figure 6.4 Flow patterns of horizontal micro-finned surfaces with 3 different fin lengths at moderate heat flux region.

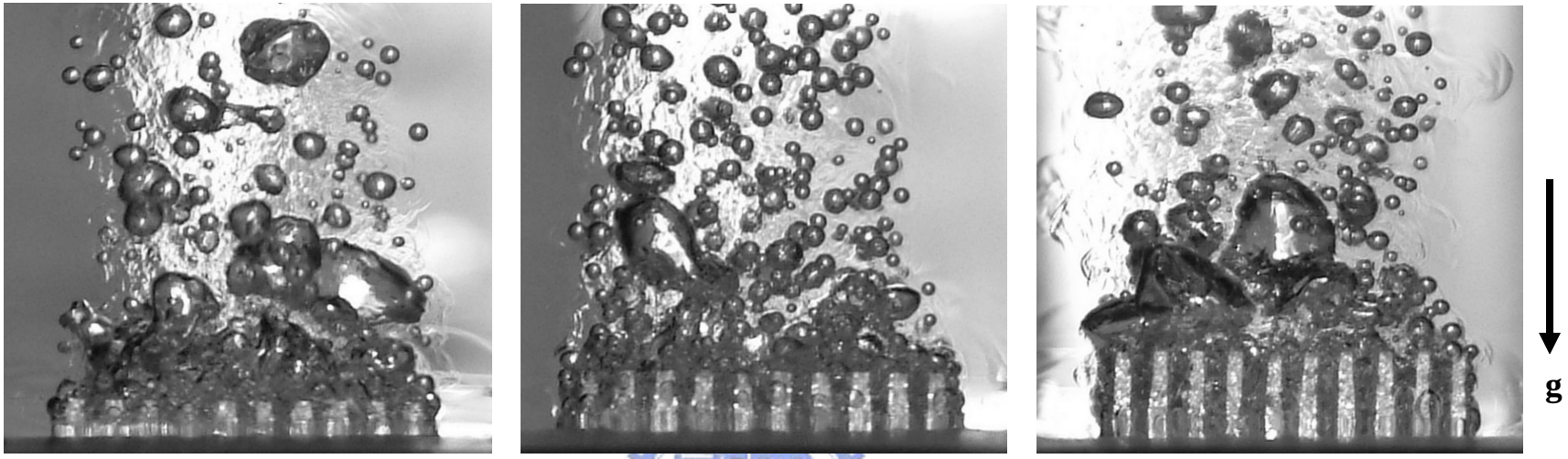

(a) L=0.5mm, 63.5% of CHF (b) L=1.0mm, 61.6% of CHF (c) L=2.0mm, 64.2% of CHF

Figure 6.5 Flow patterns of horizontal micro-finned surfaces with 3 different fin lengths at high heat flux region.

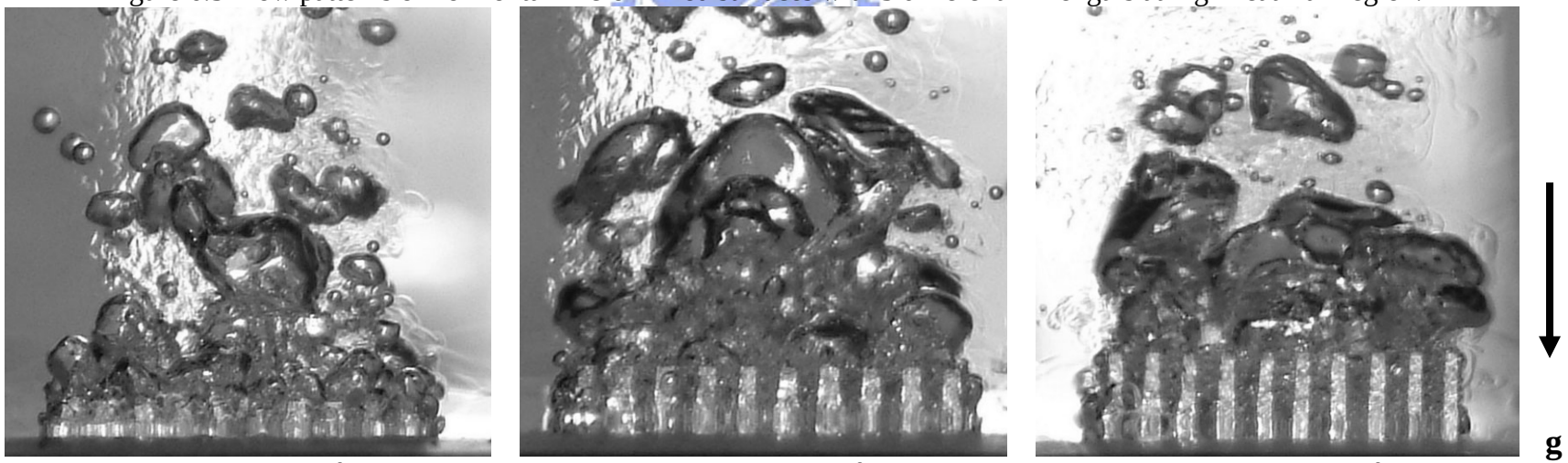

(a) L=0.5mm, 87.2% of CHF (b) L=1.0mm, 87.0% of CHF (c) L=2.0mm, 88.4% of CHF

Figure 6.6 Flow patterns of horizontal micro-finned surfaces with 3 different fin lengths at high heat flux region approach to CHF.

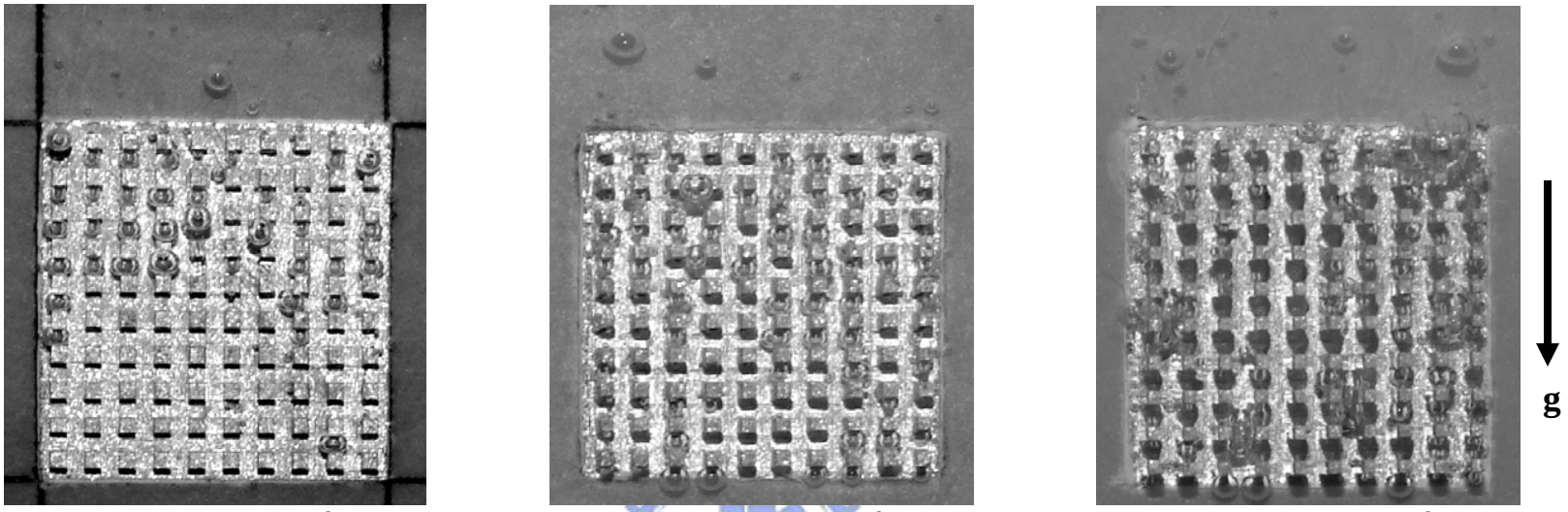

(a) L=0.5mm, 1.9% of CHF (b) L=1.0mm, 1.2% of CHF (c) L=2.0mm, 1.0% of CHF

Figure 6.7 Flow patterns of vertical finned surfaces with 3 different fin lengths at boiling incipience.

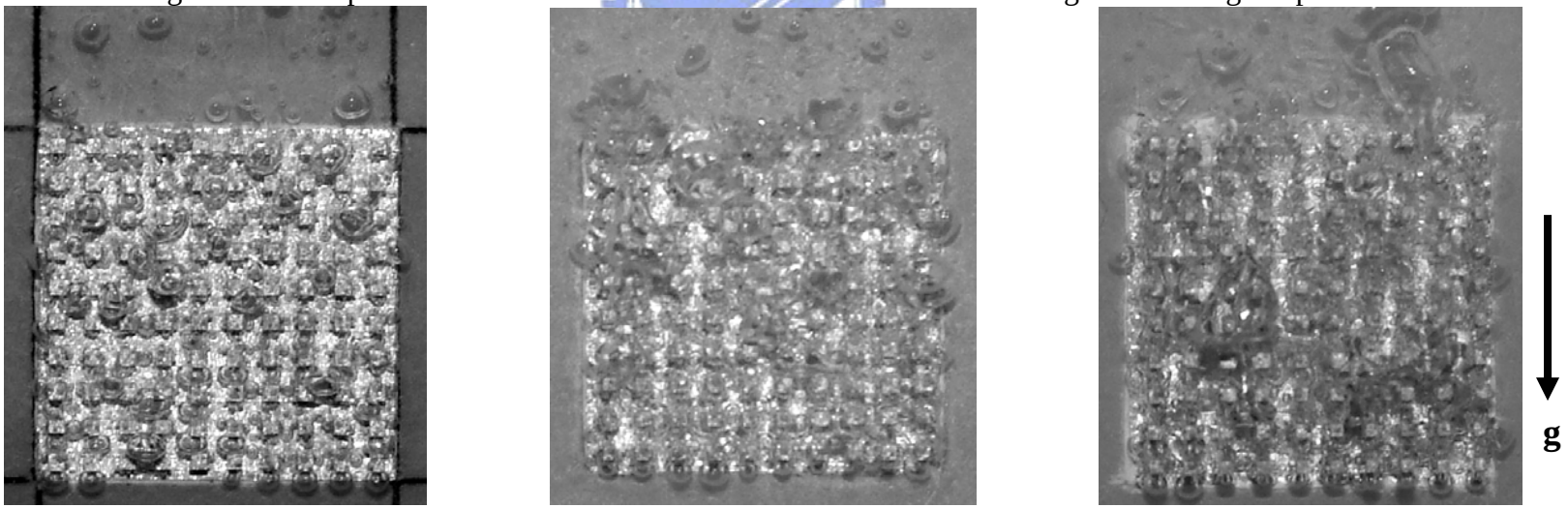

(a) L=0.5mm, 38.9% of CHF (b) L=1.0mm, 36.6% of CHF (c) L=2.0mm, 38.2% of CHF

Figure 6.8 Flow patterns of vertical finned surfaces with 3 different fin lengths at low heat flux region.

(a) L=0.5mm, 54.3% of CHF (b) L=1.0mm, 55.8% of CHF (c) L=2.0mm, 53.1% of CHF

Figure 6.9 Flow patterns of vertical finned surfaces with 3 different fin lengths at moderate heat flux region.

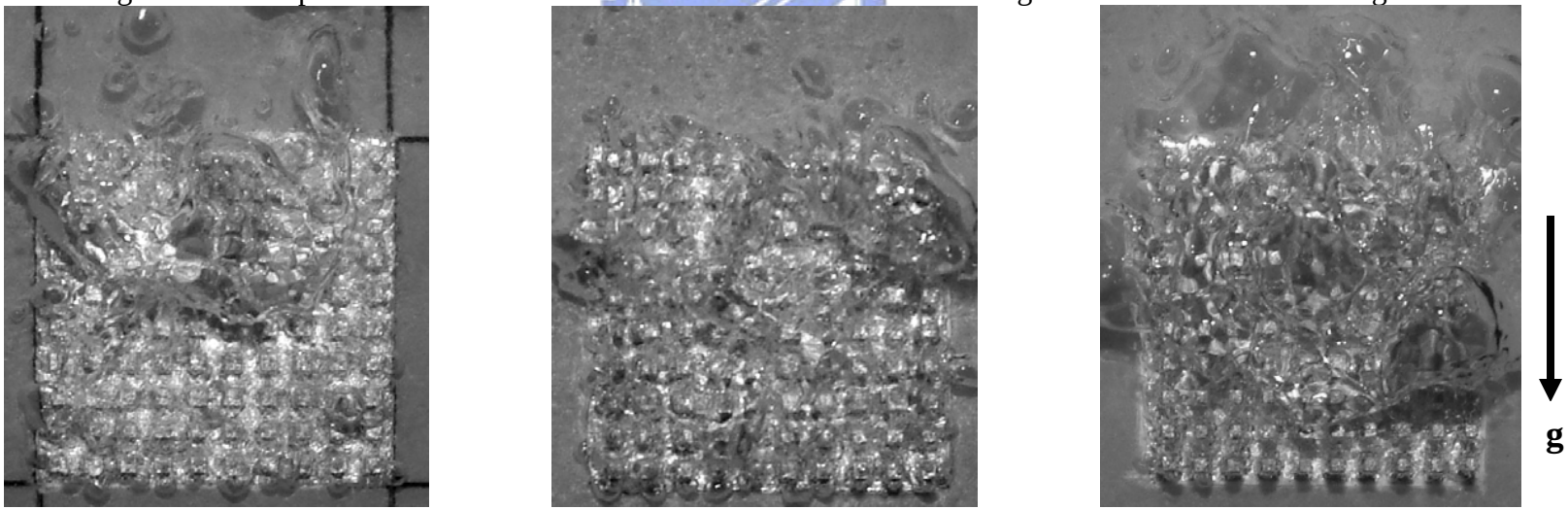

(a) L=0.5mm, 85.1% of CHF (b) L=1.0mm, 86.3% of CHF (c) L=2.0mm, 84.8% of CHF

Figure 6.10 Flow patterns of vertical finned surfaces with 3 different fin lengths at high heat flux region approach to CHF.

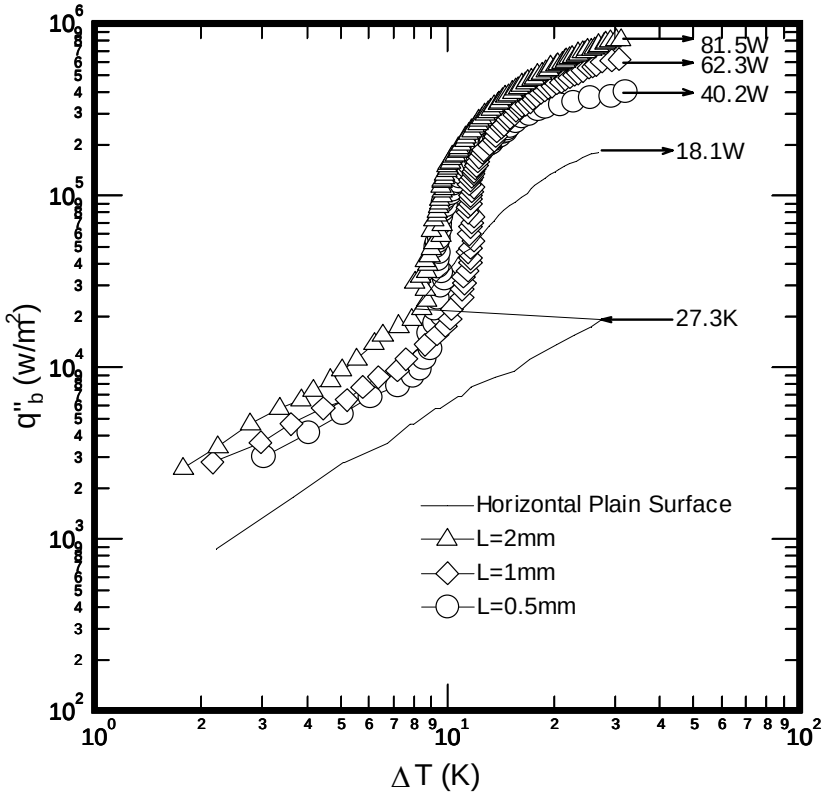

Figure 6.11 Boiling curves of micro-finned surface in horizontal orientation (Increasing heat flux).

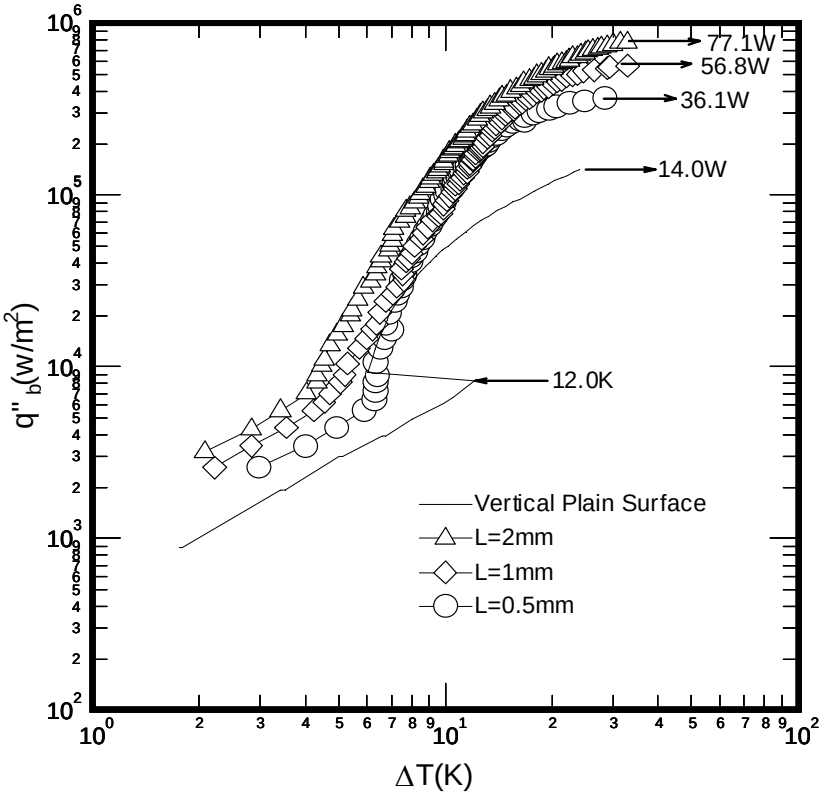

Figure 6.12 Boiling curves of micro-finned surface in vertical orientation (Increasing heat flux).

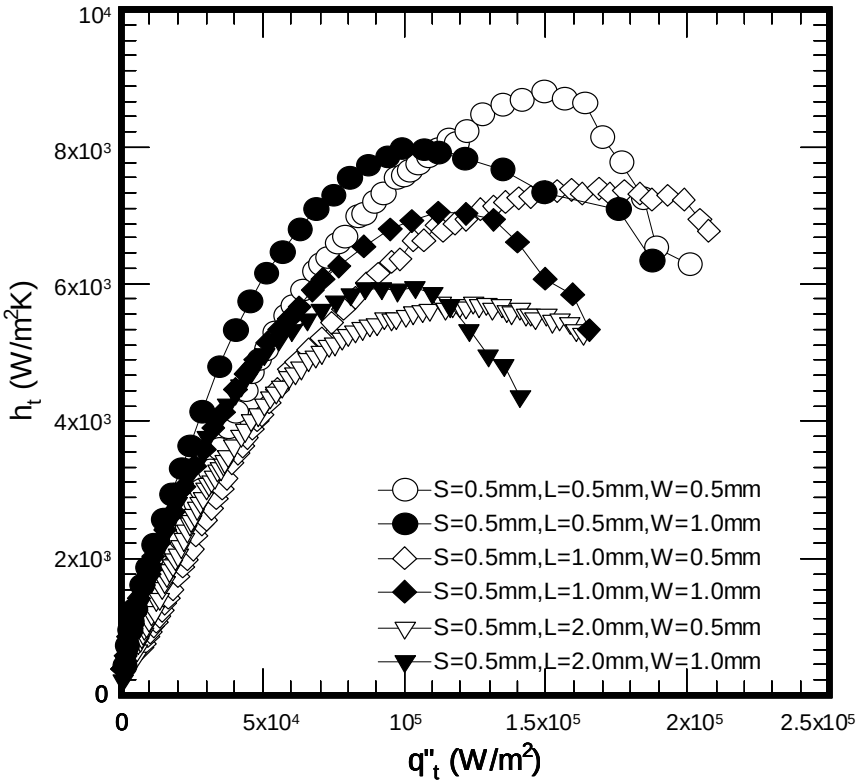

Figure 6.13 Pool boiling heat transfer coefficient with heat flux for various fin length and width in horizontal orientation.

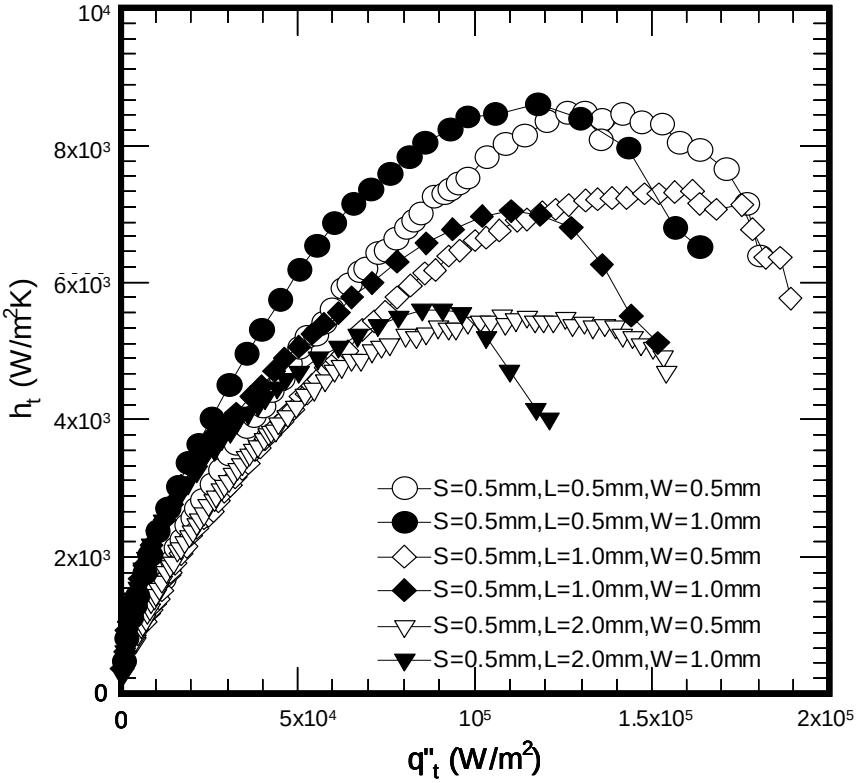

Figure 6.14 Pool boiling heat transfer coefficient with heat flux for various fin length and width in vertical orientation.

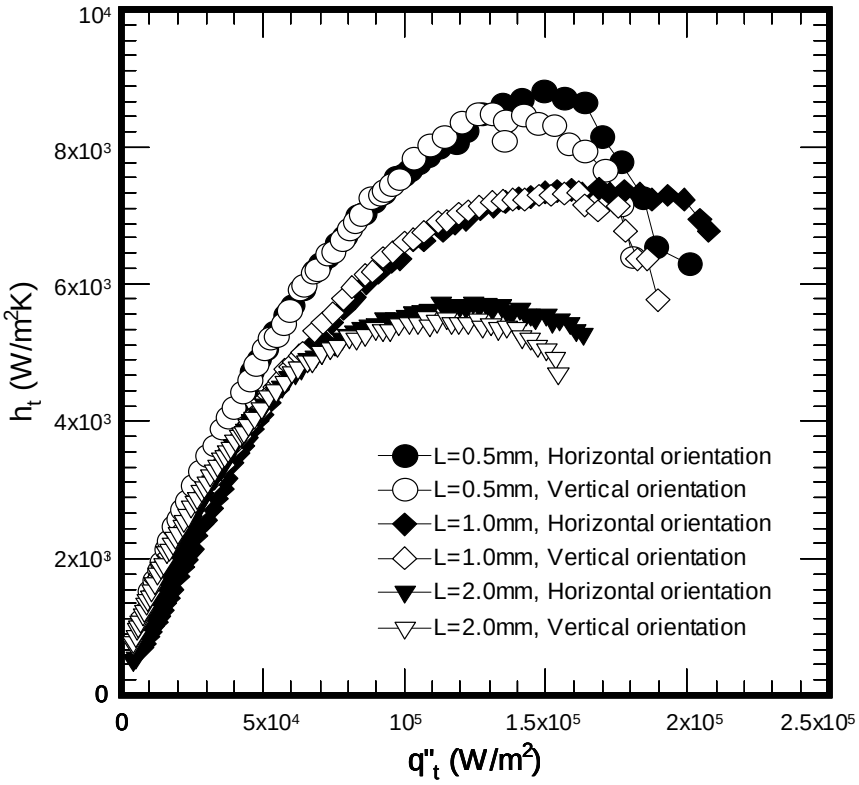

Figure 6.15 Variations of pool boiling heat transfer coefficient with heat flux for various fin length with horizontal and vertical orientation (Decreasing heat flux).